



Multilayered thin films from poly(amido amine)s and DNA



Sry D. Hujaya, Johan F.J. Engbersen*, Jos M.J. Paulusse*

Department of Controlled Drug Delivery, MIRA Institute for Biomedical Technology and Technical Medicine, Faculty of Science and Technology, University of Twente, P.O. Box 217, 7500 AE Enschede, The Netherlands

ARTICLE INFO

Article history:

Received 23 October 2014
Received in revised form 7 April 2015
Accepted 16 April 2015
Available online 27 April 2015

Keywords:

Multilayered thin films
Layer-by-layer assembly
Transfection
Gene delivery
Biodegradable polymers

ABSTRACT

Dip-coated multilayered thin films of poly(amido amine)s (PAAs) and DNA have been developed to provide surfaces with cell-transfecting capabilities. Three types of PAAs, differing in side chain functional groups, were synthesized and characterized for their properties in forming multilayered structures with ultrasonicated calf thymus DNA (CTDNA) as model DNA. All three polymers display a multilayer build-up in linear profiles as demonstrated by UV spectroscopy. More highly charged side chains were found to provide the lowest deposition of DNA. Surface profiles of the obtained films were investigated by atomic force microscopy (AFM) and static water contact angle measurements to reveal complete surface coverage after at least four layer pair depositions, where alternating patterns of surface profiles were observed depending on whether the cationic polymer or the anionic DNA layer was on top. The stability of the formed surfaces was investigated *in vitro* under physiological and reductive conditions. Owing to the presence of disulfide bonds in the PAA main chain, the films were readily degraded in the presence of 1 mM of DTT *in vitro*. Under non-reductive physiological conditions, two of the thicker films underwent thermodynamic rearrangement, which resulted in release of approximately half of the incorporated material within 1 h, which was caused by the physiological salt concentration. Further, this unpacking phenomenon proved useful in transfecting COS-7 cells seeded on top of these multilayers containing functional plasmid DNA encoding for green fluorescence protein (GFP). Two out of the three different multilayers facilitated good COS-7 cell attachment, proliferation, and transfection *in vitro* within 2 days of culture. Fluorescence staining further revealed the presence of DNA-containing released film material among cultured cells. The present work demonstrates the possibility of coating surfaces with thin films that are conveniently adjustable in thickness and amount of active agent to provide cell-transfecting functionality. In this manner transfection can be achieved by simply culturing cells on a multilayer-coated surface in their optimal culture condition (in the presence of serum) and without the need of removing the transfection agent to avoid cytotoxicity.

© 2015 Acta Materialia Inc. Published by Elsevier Ltd. All rights reserved.

1. Introduction

Multilayered thin films containing functional DNA have been of great interest during the past two decades in parallel to the ever-growing interest in the layer-by-layer (LbL) assembly technique in various fields [1]. The possibility to fabricate intricate multilayered structures within nanometer range precision, combined with the versatility of the fabrication technique, have made LbL assembly in the biomedical field an interesting option to easily modify the surface of biomedical devices [2], not only to enhance their performance but also to add additional functionality for therapeutic effect.

Due to the inherent properties of DNA as a natural biological compound, multilayers containing DNA have been investigated

for their possibility of providing relatively low-immunogenic coatings [3] and surface-mediated cell transfection on various substrates [4–7]. Multilayers containing a top DNA layer have shown a significant increase in primary rat dermal fibroblast proliferation as compared to non-coated glass surfaces *in vitro*, while *in vivo* tissue response studies also showed that the DNA-coatings are histocompatible without showing signs of inflammation or adverse reactions [3]. The current study does not concern the CpG oligodeoxynucleotides (CpG ODN) known to be immunostimulants [8,9]. The DNA used for *in vitro* viability and transfection efficiency experiments is of plasmidic nature.

Another key parameter in multilayered systems containing DNA is the polyelectrolyte counterpart. Natural polyelectrolytes such as chitosan [10] as well as synthetic polymers such as polyethyleneimine (PEI) [11] and polyallylamine hydrochloride (PAH) [12] have been successfully incorporated into multilayered systems complementing also their widely studied potency in forming polyplexes

* Corresponding authors. Tel.: +31 53 489 2926; fax: +31 53 489 2155.

E-mail addresses: J.F.J.Engbersen@utwente.nl (J.F.J. Engbersen), J.M.J.Paulusse@utwente.nl (J.M.J. Paulusse).

with DNA. Multilayers composed of DNA with more than a single type of polyelectrolyte have also been developed where highly-studied polyelectrolytes such as PEI, PAH, and polystyrene sulfonate (PSS) are used mostly for their well-known ability to form stable precursor layers [13,14] or to provide further distinction in the multilayer architecture and/or enhanced stability [15]. In addition to directly depositing DNA from a DNA solution, optimized cellular uptake of functional DNA has also been achieved by packing DNA in a liposome system [16,17] or precomplexing DNA with known polyelectrolytes such as PEI and chitosan to form a polyplex prior to the deposition step [18,19].

Poly(amido amine)s (PAA) denote a class of biodegradable polymers, which has been shown to be able to complex biotherapeutics such as proteins [20], plasmid DNA (pDNA) [21–23], and small interfering RNA (siRNA) [24] with relatively lower toxicity as compared to the standard PEI. The inherent peptidomimetic structure provides these polymers with biocompatibility and degradability while the presence of amines provides the necessary positive charges for the interaction with DNA. Furthermore, the versatility of the synthesis and possibilities to incorporate a wide variety of functionalities make this class of polyelectrolyte an interesting choice to be used in LbL assembly with DNA.

A special property of bio-reducible PAAs in relation to the intended applications as bioactive surfaces, relies on the finding that cell membranes have reductive properties owing to the presence of reducing enzymes and thiol groups in proteins present in the cell membrane [25,26]. This has triggered attempts to achieve a localized controlled release of active agents from bio-reducible multilayered thin films. Delivery of DNA in this respect is particularly interesting as there have been many attempts at surface-mediated cell transfection even without incorporation of a multilayer structure [27–29] as pioneered by the group of Oupický [30,31].

On another note, multilayered coatings may also be viewed as a delivery system that releases therapeutic agents, in the sense similar to a hydrogel, for example. Therapeutic agents to be released are incorporated during multilayer assembly and are subsequently released either via simple diffusion [32], biodegradation of the polyelectrolyte building block [33], or induced by internal [34] or external [35] triggers. In view of cell transfecting surfaces, Lynn and Bechler reported that the two multilayer components (i.e., hydrolysable poly(β -amino ester) and DNA) were found to co-localize within transfected cells cultured in the vicinity of the surface, indicating that either the polymer–DNA complex is released, or the separate components are released and later form a complex in cell culture medium before being internalized by cells [36].

Here we present the syntheses of three PAAs and the characterization of their properties in forming multilayered thin films with ultrasonicated calf thymus DNA (CTDNA) as model DNA. The effects of structural differences among the three polymers have been evaluated for their properties to form multilayers that could act as bioactive surfaces. Release profiles were studied based on the relative DNA content within the constructs under physiological conditions and in reducing environment. Finally the ensembles containing reporter plasmid pCMV-GFP (i.e., pDNA encoding green fluorescence protein (GFP)) were assessed for their efficacy in surface-mediated cell transfection of COS-7 cells.

2. Materials and methods

N,N'-cystaminebisacrylamide (CBA, 99.9%) was purchased from Polysciences (Eppelheim, Germany). 4-amino-1-butanol (ABOL, 98.0%), *N*-Boc-1,4-diaminobutane (NBDAB, $\geq 97.0\%$), histamine dihydrochloride (HIS-2HCl, $\geq 99.0\%$), calcium chloride (CaCl₂, $\geq 93.0\%$), triethylamine (TEA, $\geq 99.0\%$), *tert*-butylamine (*t*BA, $\geq 99.5\%$), trifluoroacetic acid (TFA, $\geq 99.0\%$), sodium chloride

(NaCl, $\geq 99.5\%$), calf thymus DNA sodium salt (CTDNA, type 1, fibers, 16.7 A260 unit/mg solid, 6.0% sodium), dithiothreitol (DTT, $\geq 99.0\%$), sulfuric acid (H₂SO₄, 95–98%), and hydrogen peroxide (H₂O₂, 30 wt.% in H₂O) were purchased from Sigma–Aldrich (Zwijndrecht, The Netherlands). Sodium dihydrogen phosphate monohydrate (NaH₂PO₄·H₂O, 99.0–102.0%) and disodium hydrogen phosphate dihydrate (Na₂HPO₄·2H₂O, 99.5%) were purchased from Merck (Darmstadt, Germany). All reagents and solvents were purchased at the highest purity available and used as received. Milli-Q water (18.2 M Ω cm at 25 °C) was obtained from a Synergy® water purification system (Millipore).

PBS buffer was prepared by dissolving 1.54 g of Na₂HPO₄·2H₂O, 0.30 g of NaH₂PO₄·H₂O, and 8.20 g of NaCl into 1.00 L of Milli-Q water and adjusting the pH to 7.4.

CTDNA solution in water was prepared by dissolving shredded CTDNA into Milli-Q water to the final concentration of 1.0 mg/mL. The solution was placed in an ice bath and then sonicated (Sonoplus HD2070, Bandelin, Berlin, Germany) for 20 min at 10% power, 20 kHz frequency, and 7 cycles (i.e., 0.7 s of active interval followed by 0.3 s of passive interval).

¹H NMR spectra were recorded on an AVANCE III-400 MHz NMR (Bruker, Wormer, The Netherlands) spectrometer. Gel permeation chromatograms were recorded on a Polymer Labs GPC 220 in 0.1 M NaOAc buffer pH 4 with 25% methanol as eluent and 0.7 mL/min flow rate against poly(ethylene glycol) (PEG) standards.

Ultraviolet (UV) characterization of multilayered thin films was performed in the dry state using a UV-2401 PC (Shimadzu, 's-Hertogenbosch, The Netherlands). Each film fabricated on UV-transparent 7.5 × 37 × 1 mm quartz glass (Ted Pella, Redding, USA) was measured in three different arbitrary positions. Absorbance scan was carried out in the 200–400 nm wavelength range. All data points were then corrected for baseline offset by subtracting the absorbance value at 400 nm from each data point. Relative absorbance values were obtained by normalizing each data point with the respective value at time 0.

AFM characterization was performed on a Multimode AFM (Bruker, Wormer, The Netherlands) with Nanoscope IV controller in contact mode using an MSCT cantilever with moderate spring constant of 0.5 N/m. Multilayered thin film samples were fabricated on 100 mm single side polished silicon wafer (*n*-type, 525 μ m thick, MESA+NanoLab, Enschede, The Netherlands) diced into 7.5 × 32 mm pieces.

Contact angle measurements were performed on a Krüss G10 (KRÜSS, Hamburg, Germany) contact angle measuring instrument.

Poly-D-lysine-coated 96 well plates (PDL-TCPs) for multilayer build-up for cell culture and transfection experiments were purchased from Greiner (Alphen aan den Rijn, The Netherlands). pCMV-GFP pDNA reporter gene (3487 bp) was purchased from PlasmidFactory (Bielefeld, Germany) at 1.0 mg/mL concentration in water for injection (WFI).

COS-7 cells (European Collection of Animal Cell Cultures (ECACC) Catalog No. 87021302) were grown in DMEM containing 4.5 g/L glucose and GlutaMAX™ (Invitrogen, Breda, The Netherlands) supplemented with 2% (v/v) PennStrepp (Lonza, Breda, The Netherlands) and 10% (v/v) fetal bovine serum (Lonza, Breda, The Netherlands).

Cell imaging was performed at 4 \times , 10 \times , 20 \times , and/or 40 \times objectives using an EVOS digital inverted microscope (EMS, Wageningen, The Netherlands) equipped with GFP, RFP and DAPI light cubes for expressed GFP, EthD-1, and Hoechst 33258 fluorescence imaging, respectively. EthD-1 and Hoechst 33258 were purchased from Invitrogen (Breda, The Netherlands) and Aldrich, respectively.

Fluorescence intensity measurement was carried out in an Infinite M200 PRO plate reader (Tecan, Giessen, The Netherlands). AlamarBlue for cell viability measurements was purchased from Invitrogen (Breda, The Netherlands).

2.1. Synthesis of p(CBA–DAB)

N,N'-cystaminebisacrylamide (1.01 g; 3.89 mmol) and *N*-Boc-1,4-diaminobutane (0.73 g; 3.84 mmol) were mixed in a brown polymerization flask using 2 mL of methanol/water 3/1 as solvent and containing 200 mM CaCl₂ as catalyst based on a recent report by Zintchenko et al. [37]. Polymerization was carried out under N₂ atmosphere for 3 days at 70 °C during which a gradual viscosity increase was observed. The polymerization was terminated by adding excess *tert*-butylamine (1.3 mL; 12.3 mmol) into the mixture and stirring at 70 °C for two more days. After bringing the flask to room temperature, the solution was diluted and acidified to pH ~5 by the addition of 4 M HCl and purified by ultrafiltration using a 1000 Da MWCO membrane. The purified polymer solution was then freeze-dried leaving a white foam-like solid as the final product in its HCl-salt form (1.06 g; 60% recovery). ¹H NMR spectroscopy confirmed complete termination.

Deprotection of the BOC-amino side groups in the polymer was carried out by dissolving the polymer in a mixture of methanol/TFA over the course of 1 day. The solution was then brought to pH ~5 by the addition of 1 M NaOH, filtered through a filter paper and dialyzed using a 1000 Da MWCO. The purified polymer solution was finally freeze-dried to yield a white transparent solid as the final product in its HCl-salt form (0.24 g; 23% recovery). ¹H NMR spectroscopy confirmed complete deprotection and allowed determination of the number-average MW based on the *tert*-butylamine end-group. ¹H NMR (D₂O) δ (ppm) = 1.36 (s, 9H, (CH₃)₃R); 1.75 (m, 2H, CH₂CH₂NH₂); 1.86 (m, 2H, CH₂CH₂NR); 2.81 (t, 4H, CH₂CONHRNHCOCH₂); 2.86 (t, 4H, CH₂SSCH₂); 3.05 (t, 2H, CH₂NH₂); 3.29 (t, 2H, NH₂(CH₂)₃CH₂NR); 3.47 (t, 4H, NCOCH₂CH₂NRCH₂); 3.53 (t, 4H, CH₂CH₂SSCH₂CH₂).

2.2. Synthesis of p(CBA–ABOL)

N,N'-cystaminebisacrylamide (0.53 g; 2.04 mmol) and 4-amino-1-butanol (0.19 g; 2.06 mmol) were mixed in a brown polymerization flask using 1 mL of methanol/water 3/1 as solvent and containing 200 mM CaCl₂ as catalyst [37]. Polymerization was carried out under N₂ atmosphere for 2 days at 70 °C during which a gradual viscosity increase was observed. The polymerization was terminated by adding excess *tert*-butylamine (0.7 mL; 6.63 mmol) into the mixture and stirring at 70 °C for three more days. After bringing the flask to room temperature, the solution was diluted and acidified to pH ~5 by the addition of 4 M HCl and purified by ultrafiltration using a 1000 Da MWCO membrane. The purified polymer solution was then freeze-dried leaving a white transparent solid as the final product in its HCl-salt form (0.39 g; 50% recovery). ¹H NMR spectroscopy confirmed complete termination and allowed determination of the number-average MW based on the *tert*-butylamine end-group. ¹H NMR (D₂O) δ (ppm) = 1.35 (s, 9H, (CH₃)₃R); 1.60 (m, 2H, CH₂CH₂NR); 1.77 (m, 2H, CH₂CH₂OH); 2.74 (t, 4H, CH₂CONHRNHCOCH₂); 2.85 (t, 4H, CH₂SSCH₂); 3.22 (t, 2H, HO(CH₂)₃CH₂NR); 3.44 (t, 4H, NCOCH₂CH₂NRCH₂); 3.53 (t, 4H, CH₂CH₂SSCH₂CH₂); 3.62 (t, 2H, CH₂OH).

2.3. Synthesis of p(CBA–HIS)

N,N'-cystaminebisacrylamide (1.24 g; 4.74 mmol) and histamine dihydrochloride (0.88 g; 4.75 mmol) were mixed in a brown polymerization flask using 2.3 mL of methanol/water 3/1 as solvent and containing 200 mM CaCl₂ as catalyst [37]. Triethylamine (3.3 mL, 23.0 mmol) was added to free the primary amine of histamine dihydrochloride. Polymerization was carried out under N₂ atmosphere for 2 days at 70 °C during which a gradual viscosity increase was observed. The polymerization was terminated by adding excess *tert*-butylamine (1.5 mL; 14 mmol)

into the mixture and stirring at 70 °C for two more days. After bringing the flask to room temperature, the solution was diluted and acidified to pH ~5 by the addition of 4 M HCl and purified by ultrafiltration using a 1000 Da MWCO membrane. The purified polymer solution was then freeze-dried leaving a white transparent solid as the final product in its HCl-salt form (1.14 g; 54% recovery). ¹H NMR spectroscopy confirmed complete termination and allowed determination of the number-average MW based on the *tert*-butylamine end-group. ¹H NMR (D₂O) δ (ppm) = 1.39 (s, 9H, (CH₃)₃R); 2.78–2.95 (m, 8H, CH₂CONHRNHCOCH₂ & CH₂SSCH₂); 3.23 (t, 2H, CCH₂); 3.48–3.80 (m, 10H, (CH₂)₃N & CH₂CH₂SSCH₂CH₂); 7.45 (s, 1H, NC=CH); 8.71 (s, 1H, N=CH).

2.4. Multilayered thin film construction and build-up profiles

Fresh PAA solutions were prepared short before the start of multilayer build-up from the solid materials which had been re-lyophilized overnight to avoid weighing errors due to their hygroscopic properties. All PAA solutions (2.0 mg/mL) were prepared in PBS buffer at pH 7.4 to avoid possible variations in pH. All CTDNA solutions (1.0 mg/mL) in Milli-Q water were prepared from a single batch.

Prior to the assembly, quartz or silicon wafer substrates (7.5 mm × 32 mm) were etched for 30 min in piranha acid solution to activate the surface, rinsed with copious amounts of Milli-Q water, and dried under N₂ stream. These substrates were then dipped into PAA solution (2.0 mg/mL in PBS buffer pH 7.4) for 10 min, transferred into washing solution containing PBS buffer for 1 min, dipped briefly in a large amount of Milli-Q water, transferred into CTDNA (1 mg/mL in Milli-Q water) solution for 10 min, dipped into the second washing solution containing Milli-Q water for 1 min, and finally followed by another brief dipping in Milli-Q. This cycle was repeated to reach the desired number of bilayers. Drying under N₂ stream was performed after every PAA-layer deposition, excluding the very first layer. The resulting ensemble is denoted by PAA-(CTDNA#PAA)_{*n*}, where PAA represents the identity of the poly(amido amine) used and *n* represents the number of the bilayer. The first PAA layer is regarded as a precursor layer and therefore excluded from the bilayer number count. Typically, the ensemble consists of 10 bilayers with the poly(amido amine) polymer as the last layer. For every multilayered system, three samples were fabricated in parallel to give an estimation for standard deviation. To study the build-up profiles, UV spectra were recorded after each drying step. Afterward, the multilayers were dipped into CTDNA solution to continue multilayer build-up.

Multilayers for cell culture were fabricated directly in the wells of poly-D-lysine-coated 96-well plates (PDL-TCPS, Greiner) by alternately dispensing deposition (70 μL) and washing (2 × 100 μL) solutions under sterile conditions inside the laminar flow hood (LFH). Deposition started with pCMV-GFP (1 mg/mL, 30 min for the first layer, 10 min next) as the first layer to a total of 10 bilayers ending with the PAA layer. No intermediate drying steps were applied. At the end of the fabrication the plates were left inside the LFH briefly to dry the films. Coated plates were kept at 4 °C and used as soon as possible (typically overnight). These multilayered samples are designated as PDL-(pCMV-GFP#PAA)₁₀ to indicate the presence of a PDL layer as a precursor layer. Compared to multilayers built on quartz and silicon wafer substrates, these systems substitute the first PAA layer with PDL layer inherent to the well plate surface.

2.5. Contact angle measurements

Static contact angles (*θ*) were measured with Milli-Q water (18.2 MΩ cm) on a Krüss G10 Contact Angle Measuring Instrument. Five drops of Milli-Q water (approximately 1.5 μL) were

measured on five different spots across the surface and averaged to obtain θ . Images were recorded and measured for θ approximately 15 s from the initial contact of the liquid and the surface.

2.6. Atomic force microscopy

Multilayers built on silicon wafer substrates were used for AFM microscopy. Imaging was carried out in the middle part of the films (to avoid edge effects/defects) at three different $20 \times 20 \mu\text{m}$ scan areas at 512×512 pixels. Images were taken and analyzed using Nanoscope software version 7.30. Height data was flattened using first or second order fitting and root mean square roughness (RMS) was calculated over the scan area. Thickness data were obtained by first scratching the surface using a syringe needle and then scanning over the scratched area to measure the difference in height between the base substrate (i.e., the bottom of the scratch) and the surface of the film. Thicknesses were then measured as the average of one 'depth' measurement and three 'section' measurements across the scratch.

2.7. PicoGreen assay

An indirect PicoGreen assay was performed to determine the DNA-content in multilayers. Multilayered samples were prepared as described above. After multilayer formation, pCMV-GFP and PAA deposition solutions were collected and diluted 500 times in sterile water. A pCMV-GFP solution with known concentration was used for calibration purposes. Diluted solutions ($10 \mu\text{L}$) were transferred into a black 96-well plate containing $1 \times$ PicoGreen solution ($90 \mu\text{L}$) in TE buffer, incubated for 5 min at RT in the dark and analyzed for fluorescence intensity (485/520 ex/em) using the Infinite M200 PRO plate reader (Tecan, Giessen, The Netherlands).

2.8. DNA release profiles under physiological conditions

DNA release profiles of the three multilayered systems in PBS buffer pH 7.4 at 37°C were investigated by dipping the thin films formed on quartz slides in 2 mL of PBS buffer pH 7.4 solution and incubating them in a water bath with the temperature set to 37°C . From time to time, the samples were removed, briefly dipped in a large amount of Milli-Q water, dried under N_2 stream and measured by UV-Vis spectrophotometry.

2.9. DNA release profiles under reducing conditions

Degradability of the three multilayered systems was investigated in a similar fashion as for their DNA release profiles under physiological conditions, though in the presence of 1 mM of DTT in the incubation medium. The solution of 1 mM DTT in PBS buffer pH 7.4 was prepared fresh directly prior to the start of experiment. Due to instability of DTT in PBS buffer pH 7.4, no solution of over 3 h old was used.

2.10. Cell viability and transfection on multilayered films

For cell viability and transfection experiments, multilayers were fabricated as described before. Directly on the multilayer-coated PDL-TCPS wells, COS-7 cells were seeded at a seeding density of 4500 cells/sample in complete medium with serum and left to proliferate at 37°C in humidified atmosphere with 5% CO_2 .

Cell morphology and transfection efficiency were recorded after 6, 24 and 48 h of culture. At the end of the 2 day culture period, cells were stained with EthD-1 and Hoechst 33258 followed by subsequent fluorescence imaging. As (negative for transfection and positive for metabolic activity) controls, cells were also seeded

on non-TC-treated, polystyrene well plates. Experiments were done in triplicate.

For quantitative metabolic activity comparison between the three different polymer systems, after 48 h of culture, AlamarBlue (AB) was added at 10 v/v% of total medium volume in every well and incubated for another 4 h after which fluorescence intensity of resorufin (i.e., metabolically-reduced resazurin) was recorded using a plate reader. As positive controls, cells were also seeded on non-TC-treated polystyrene well plates. All fluorescence intensities were corrected by subtracting the values with those of their respective no-cell control wells. All experiments were carried out in triplicate.

To study the effect of burst release of thicker multilayers on transfection efficiency, cells were seeded on pCHIS films which had and had not been previously washed by incubating in PBS buffer pH 7.4 inside the incubator for 1 h. The extent of transfection efficiency was assessed qualitatively using fluorescence imaging.

2.11. Statistical analysis

Data were analyzed and plotted with the GraphPad Prism (Version 6.01) software. All data points were expressed as the mean \pm standard deviation (SD). Statistical significant analysis was performed based on the *t*-test and the difference was considered to be significant when $P < 0.05$.

3. Results and discussion

3.1. Syntheses of pCDAB, pCABOL, and pCHIS

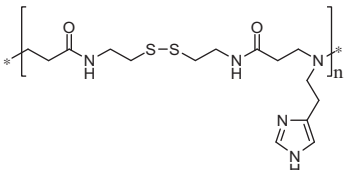
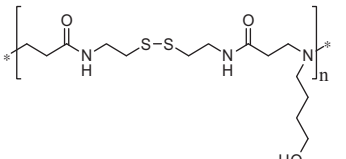
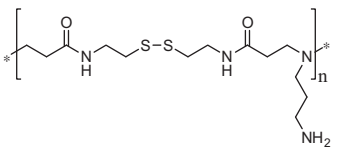
To study the effect of structural differences of the polymers on multilayer build-up, PAAs with different side chain functional groups were synthesized via CaCl_2 -catalyzed Michael-type addition polymerization (Table 1). To obtain the highest degrees of polymerization, the polymerization was performed using an equimolar mixture of free amine and bisacrylamides. Moreover, solvent was kept to a minimum amount to increase the rate of the polymerization. N_2 gas as a protective atmosphere, in combination with a brown reaction flask, was used to prevent radical formation. CaCl_2 was employed as a Lewis acid, which is known to catalyze the addition of nucleophilic amines to α,β -unsaturated carbonyl compounds [37]. All polymerizations were run for 2–3 days at 70°C to maximize the degree of polymerization, but no longer in order to avoid retro-Michael reaction and possible amide hydrolysis. Polymerizations were terminated by adding excess *tert*-butylamine (*t*BA), resulting statistically in one *t*BA end group per polymer chain, provided the ideal stoichiometry was achieved. Neutralization and dialysis were then carried out to obtain the PAA product in aqueous solution. Water was removed via lyophilization to obtain the pure polymer in its salt form. For p(CBA–DAB), an extra BOC-deprotection step was necessary, which was carried out by dissolving the dry product in a methanol/TFA mixture, which was stirred overnight at RT.

From the ^1H NMR spectra, the observed singlet corresponding to the *t*BA end group was used to make an estimation of the number-average molecular weight (M_n) for each polymer. Polydispersity index (PDI) values were obtained from GPC, together with the weight (M_w) and number (M_n) average molecular weight, relative to PEG standards. These data are shown in detail in Table 1.

The (physico-)chemical difference between the three different PAAs is mainly based on the different properties of the side chains. Under the physiological conditions applied for the build-up and application of the resulting multilayers, the primary amine in the pCDAB side chains provide additional positive charges ($\text{pK}_a \sim 9$)

Table 1

Summary of ^1H NMR and GPC characterizations on the molecular weights in kg/mol and PDI of PAA products. The number of repeat units (n) was calculated through ^1H NMR spectroscopy end group analysis.

PAA name	PAA structure	^1H NMR end group analysis		GPC (PEG standard)		
		n	M_n (kg/mol)	M_w (kg/mol)	M_n (kg/mol)	PDI
p(CBA-HIS) (pCHIS)		15	5.5	4.6	3.6	1.26
p(CBA-ABOL) (pCABOL)		26	9	3.8	3.2	1.18
p(CBA-DAB) (pCDAB)		19	6.6	7.3	5.5	1.34

for stronger electrostatic interactions with the negatively-charged DNA. As compared to the neutral primary alcohol of pCABOL, the histamine side group in pCHIS has a pKa of 5.8 which provides an intermediate pH-sensitive amount of extra positive charge as compared to pCDAB's primary amine.

As the build-up of multilayers studied here depends largely on the electrostatic interactions between the polymers and the DNA, a structure–property relationship could be derived by studying the effect of PAA identity on its build-up profiles with DNA. Additionally, these structural differences are also expected to play a role in cell attachment and cytotoxicity as it is known that materials with higher positive charges are more prone to display cytotoxicity [38]. For an optimal surface-mediated transfection, a PAA should be non-toxic, facilitate multilayer build-up, and achieve maximal transfection efficiency.

3.2. Multilayered thin films construction

Build-up profiles of each multilayer were obtained by observing the increase in absorbance of CTDNA at 260 nm after deposition of each bilayer. The topmost layer was always the PAA layer to protect the DNA and promote future cell adhesion. As shown in Fig. 1, the build-up profiles of the three multilayered systems designated as pCDAB-(CTDNA#pCDAB)₁₀, pCABOL-(CTDNA#pCABOL)₁₀, and pCHIS-(CTDNA#pCHIS)₁₀ are relatively linear. It is noted that for the pCABOL system, the build-up profile shows a slight agreement with an exponential build-up profile, as first reported by Lavalle et al [39]. However, to obtain a more definitive conclusion, further investigations into the increases in absorbance values at higher bilayer numbers are required. For the number of bilayers up to ten, pCABOL-based multilayers displayed a relatively linear build-up profile (R^2 value for linear regression = 0.9562).

For each type of film, three parallel build-up experiments were carried out to give an indication of the reproducibility of the assembly. The polymer pCDAB gave a highly reproducible multilayer formation with DNA and exhibits very low standard deviation. This trend is generally preserved even when the build-up was continued up to 30 bilayers (data not shown). On the other

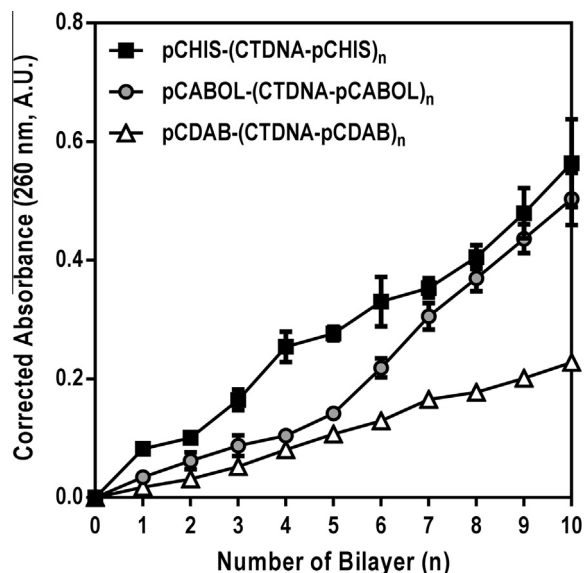


Fig. 1. Build-up profiles of three multilayers prepared using PAA-polymers with different side groups.

hand, for pCHIS and pCABOL-based multilayers, the standard deviations are generally higher, especially at higher bilayer numbers.

For pCABOL and pCHIS systems, the general trend in increase of DNA adsorption during build-up of the multilayer indicates comparable amounts of incorporated DNA. However, the two types of films possess different physical appearances. pCHIS-(CTDNA#pCHIS) multilayers often appear turbid, causing in some cases high (UV) baseline shifts, while pCABOL-(CTDNA#pCABOL) multilayers are generally more homogeneously transparent.

A PicoGreen assay was carried out to determine the DNA content within the multilayers. Respective loadings of 650, 540 and 250 ng/cm²/layer were found for the 10-bilayered pCABOL, pCHIS and pCDAB multilayers. These values correspond to 2.37, 1.96 and 0.91 μg of pCMV-GFP per well, respectively. In relating the structural differences in the three PAAs with their layer build-up

properties with DNA, it is interesting to note that the PAA with the highest cationic charge density (i.e., the pCDAB polymer) incorporates the lowest amount of DNA in each deposition cycle, while pCHIS and pCABOL result in deposition of at least twice the amount of DNA per cycle. Considering that the main interactions during multilayer build-up are electrostatic interactions, one would intuitively expect that the PAA that can interact most strongly with DNA would facilitate deposition of more DNA. Therefore, the observed phenomenon indicates that factors other than the strength of electrostatic interactions also determine multilayer build-up properties.

The much observed effects of salt concentration and pH of the deposition solution on multilayer build-up profiles have been described in the literature [40,41]. In general, the incremental thickness of adsorbed layers is found to decrease with increasing polyelectrolyte charge density. Therefore, strong polyelectrolytes are found to have higher incremental thickness only in the presence of higher salt concentration which would mask (i.e., decrease) their apparent charge density. In contrast, the incremental thickness of weak polyelectrolytes highly depends on the pH of the deposition solution which determines the extent of the polyelectrolyte's charge density. The fact that in the same deposition pH, PAA-polymers with higher charge density lead to the lowest deposition of DNA is in agreement with this trend. It is thermodynamically [42] more favorable for pCDAB, having the highest charge density, to assume a flatter conformation on the surface and therefore lower amounts of DNA are needed to compensate for surface charge reversal. On the other hand, pCABOL with less charge density would assume a conformation that is more similar to its conformation in free solution and appear more as loops on the surface (i.e., with less contact points with the surface per chain), increasing the relative surface area to facilitate more DNA deposition. This argument is also supported by the fact that the surface roughness values of pCDAB-films at various bilayer numbers (see Fig. 2) are always significantly lower than those of pCABOL-films, especially when the pCDAB is the topmost layer.

As previously indicated, compared to pCABOL, pCHIS polymer possesses a higher charge density at the deposition pH of 7.4 due to the presence of the imidazole ring with a pKa of 5.8. However, this translates to only ~2.5% of the polymer side chain to be positively-charged. Therefore, it is not surprising that the pCHIS multilayer build-up profile is much closer to that of pCABOL than pCDAB. However, as will be explained further below, the imidazole

ring induces an additional effect on multilayer build-up not yet apparent in Fig. 1.

AFM characterization was also carried out to study the build-up profiles of the different multilayers. Thickness for the single-bilayered film of pCHIS system was measured ~10 nm. For the other two polymers, the single-bilayered films were too thin to locate the scratch. The build-up profiles in terms of layer thickness were plotted in Fig. 2 and the obtained data correlates well with the UV-data shown in Fig. 1. Both thickness and absorbance values increase relatively linearly with the number of deposition cycles. The same trend is also observed for the surface roughness (RMS). It is interesting to note that RMS values of the pCHIS system were generally lower than those of the other two systems, especially considering the relatively higher thickness of the pCHIS system. This can most likely be attributed to the different interaction mechanism on which the multilayer build-up of the pCHIS system is based.

In comparing the thickness data obtained from UV absorbance with data of AFM, it is important to note that the latter gives insight in the total film thickness attributed to the two constituents of the films (i.e., the PAA polymer and the DNA) while the former can be attributed primarily to the DNA alone. The fact that the thickness of the 10-bilayered pCHIS system is approximately twice the thickness of that of the pCABOL system, while the UV absorbance values for DNA content are much closer in agreement, may indicate that the pCHIS-based film incorporates more polymer than DNA as compared to pCABOL-based films. This also agrees well with the physical appearance of pCHIS-based films, which are notably more opaque than the pCABOL-based films. Lastly, similar to the UV-spectroscopy data, AFM data also displays a considerable standard deviation, particularly for the thicker systems at higher bilayer number.

3.3. Multilayered thin film wettability

Measurement of water contact angles has often been used to indicate alternation of surface coverage in LbL assemblies [30,43]. When two (oppositely charged) materials provide different water contact angles when forming a uniform layer on a surface, alternating contact angles can be observed as multilayers of the different materials that are built-up. Fig. 3 shows contact angles of multilayers prepared with different bilayer numbers. Bilayer numbers that are integers (2, 5, 8, and 10) that represent multilayers with a PAA

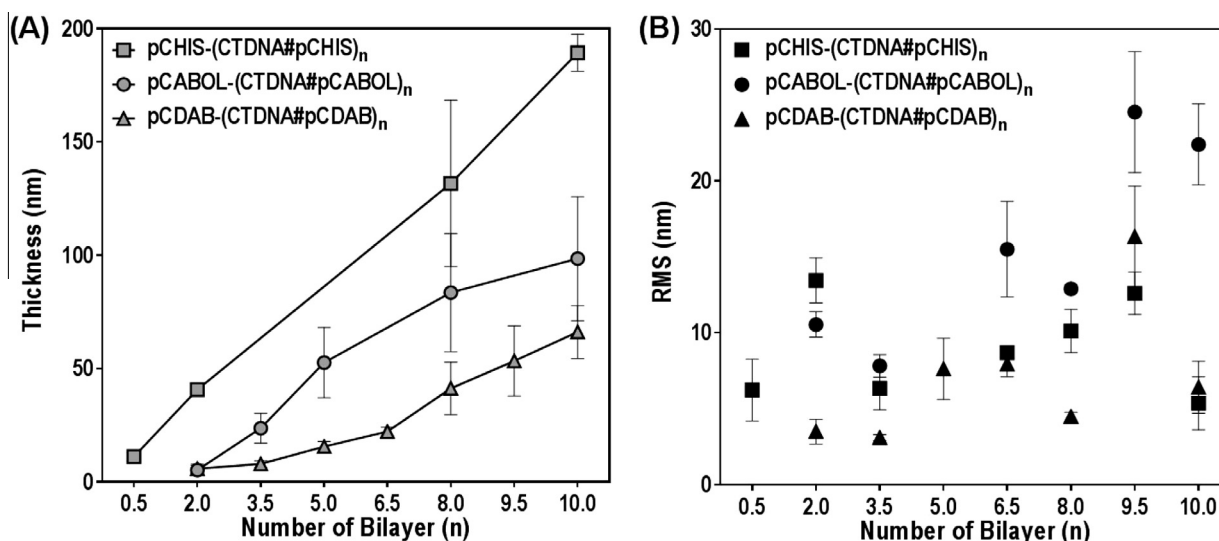


Fig. 2. Build-up profiles of the three multilayered systems based on AFM: (A) Thickness (nm) and (B) surface roughness (RMS, nm) at different bilayer numbers. Every data point is an average of at least three measurements made on arbitrary positions of the same multilayer sample.

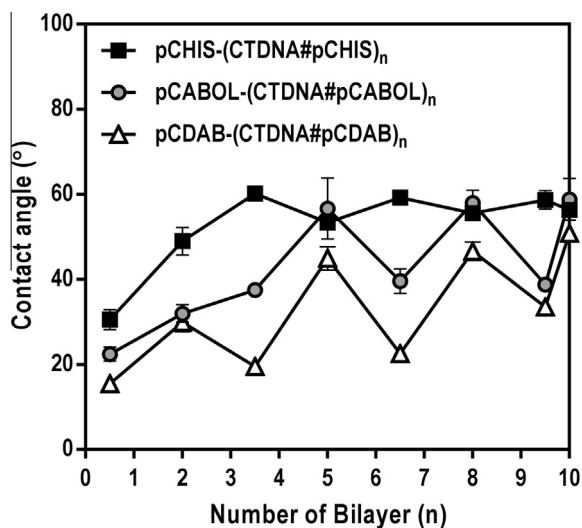


Fig. 3. Static water contact angles of multilayers with different numbers of bilayers.

layer as the outermost layer, while non-integer bilayer numbers (0.5, 3.5, 6.5, and 9.5) represent multilayers with a DNA layer as the outermost layer.

Fig. 3 indicates that the early deposition steps do not provide completely uniform layers, except for the pCDAB-(CTDNA#pCDAB) system. Complete surface coverage can be achieved after at least 4 bilayer formations, where the water contact angles now alternates between the more hydrophilic surface of CTDNA and the more hydrophobic surface of PAA. However, this phenomenon is much less pronounced for the pCHIS-(CTDNA#pCHIS) system, displaying similar water contact angles for both surfaces after the fourth bilayer. The presence of the histamine group in pCHIS leads to the formation of a more hydrophobic surface, even after DNA coverage.

As a natural amino acid, histamine has been shown to interact with DNA via both hydrogen bonding and intercalation [44]. This interaction is most likely further enhanced with the histamine moieties being the pendant group of a polymeric backbone. The topmost pCHIS layer dynamically integrates with incoming DNA resulting in a relatively hydrophobic surface. In the context of multilayer formation, this phenomenon may also indicate extensive mixing of layers resulting in a less stratified multilayer structure [45].

3.4. Multilayered thin film surface profiles

In addition to determining surface roughness, AFM was used to study the surface profiles of the various multilayered systems. Table 2 shows the surface profiles of the three different multilayers at 9.5 and 10 bilayer numbers to represent DNA and PAA topmost layers, respectively. All images are shown using the same height scale range (max z-axis 100 nm). The characteristics of the surface profiles tend to be preserved with respect to the identity of the outermost layer of the films also from the earlier bilayer numbers (data not shown). DNA topmost layers generally display sharp height differences. PAA topmost layers, on the other hand, tend to be more homogeneous with shorter and more equally-spaced elevations. This trend in alternating surface roughness is also observed from the RMS data shown in Fig. 2.

3.5. DNA release profiles under physiological conditions

Incubation of the prepared multilayers in PBS buffer pH 7.4 at 37 °C may give insight into how the films behave in physiological environment, specifically, the effect of physiological pH, salt

concentration and temperature. To be able to act as cell-transfecting surfaces, the films need to deliver transfection agents into the cells. In that respect, this study may also serve to indicate a release profile of incorporated therapeutic DNA. To approach the ideal sink conditions, after every incubation time point, the films were briefly dipped in a large amount of Milli-Q water to remove loosely attached material before being dried. The dipping solution was also refreshed after every intermitting measurement.

Fig. 4 shows the DNA release profile based on absorbance values at 260 nm normalized to 100% at time zero. The profile depicts a trend where films from PAA with higher positive charge (pCDAB-based film) seem to be more stable and retain incorporated DNA while films from PAA with less charge (pCHIS- and pCABOL-based film) tend to more rapidly release their DNA content within a few hours of incubation under physiological conditions. Despite the apparent difference, it needs to be noted that when taking into account the initial DNA content, the two multilayers with higher initial DNA content (i.e., pCHIS- and pCABOL-based films) are the ones to rapidly release their DNA content to finally reach a relatively similar DNA content level as that of the most stable multilayer (i.e., pCDAB-based film).

Since the most likely chemical degradation under the established physiological conditions is slow amide hydrolysis, the fast decrease in multilayer's 260 nm absorption can only be caused by rearrangement or disassembly of the multilayered ensembles. The possibility of disassembling multilayered systems was considered based on the fact that the burst release is observed only for the thicker films and that higher thickness may induce instability as minor defects in each layer are progressively transferred in further build-up of the layers. To verify this, 5 bilayered-pCHIS-(CTDNA#pCHIS) multilayers were built-up and incubated under the same conditions. The observed stability trend was identical to that observed for the 10-bl system (data not shown). This indicates that the burst release phenomenon is less likely caused by disassembly, but more likely thermodynamic rearrangement within the multilayered film to reach a more stable state which in turn leads to release of excess material.

The thermodynamic rearrangement is considered especially because this burst release phenomenon takes place only in the presence of physiological salt concentration. When salt was excluded in the incubation medium, all multilayers retain their DNA content in a profile similar to that of pCDAB-based film (data not shown). This leads to the argument that this phenomenon is most likely induced by two factors: deficiency of positive charges in pCABOL and pCHIS at pH 7.4 in combination with low molecular weight of the polymers. Low molecular weight leads to less multivalent interactions, promoting entropically-driven detachment from DNA on the surface, while the deficiency of positive charges makes it easier for salt ions to intervene the electrostatic interactions between the PAA and DNA. In later stages, the release of material is slowed down after the system reaches a more stable state. The presence of the charged substrate helps keep the remaining layers together, while amide hydrolysis slowly proceeds to degrade the remaining films. Similar salt-induced deconstruction has been reported previously by Ren et al. and Schüller and Caruso for DNA-containing multilayers [46,47] and others [48–50], although mostly at higher salt concentrations than 0.15 M utilized in this study.

It is noted that since the multilayers were built in the same PBS solution as that used for the incubation experiment, the rearrangement may have also been observed during layer deposition. This was most likely prevented by the presence of a high concentration of macromolecules in the deposition solutions and by the lower temperature during deposition (i.e., room temperature) as opposed to the physiological temperature used during the release experiment (i.e., 37 °C).

Table 2
Surface profiles of the three multilayered systems at 9.5 (DNA topmost) and 10 (PAA topmost) bilayer numbers scanned over $20 \times 20 \mu\text{m}$ area; max z-axis value = 100 nm.

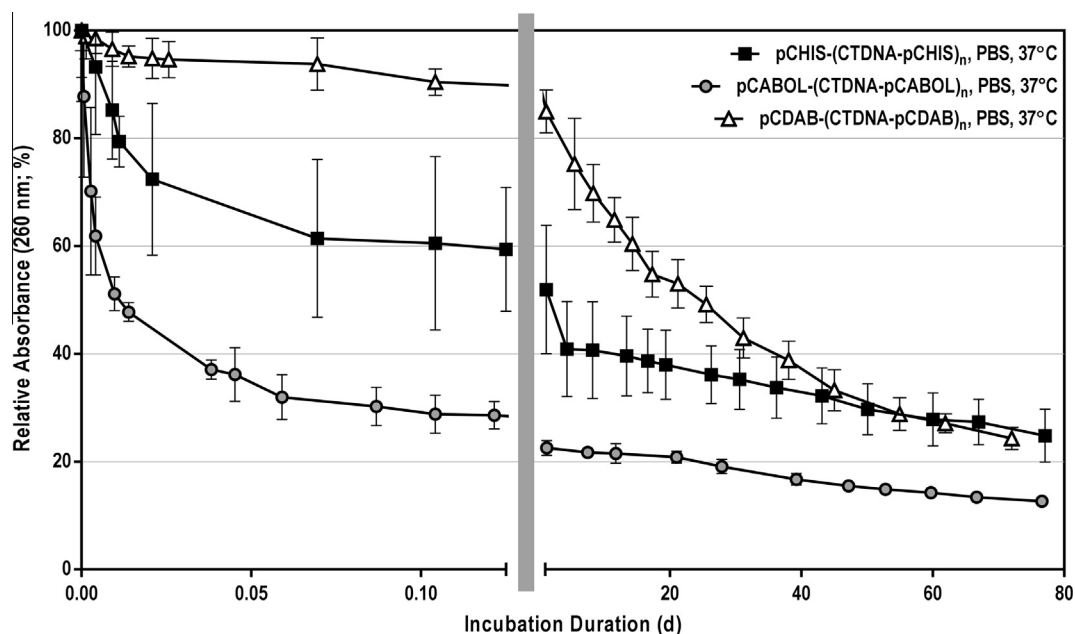
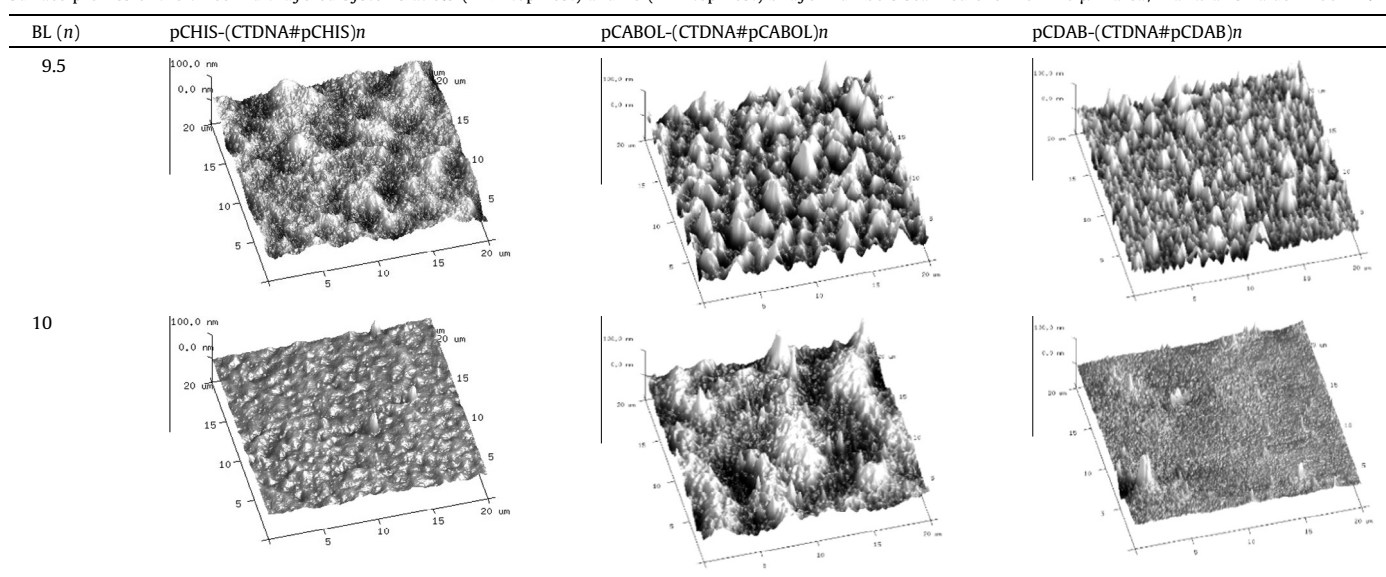


Fig. 4. DNA release profiles of multilayers under physiological conditions (PBS buffer pH 7.4 at 37 °C) *in vitro*. The left part of the abscissa shows the trend of fast decrease (burst release) within 0.125 day (3 h) in the initial phase of the incubation while the right part shows the much slower decrease throughout the rest of the long incubation duration. Relative absorbance values are shown by normalizing the absorbance values at every time point to that of time 0.

Surface profiles of the three different films at 10 bilayers, after being incubated in PBS buffer pH 7.4 at 37 °C for 1 h, are shown in Fig. 5. The surfaces were in general rougher as compared to the respective surfaces before rearrangement (roughness increases were ~40% and ~20% for pCHIS- and pCDAB-systems, respectively). Notably, the pCABOL-based system (the roughest of the three prior to incubation in PBS) showed the presence of high features most likely indicating the still-attached released complexes/aggregates of pCABOL and DNA, causing high increase in surface roughness of up to 170%. AFM scratch tests on these films revealed the expected decreases in thickness; i.e. from the original thicknesses of 190, 99, and 66 nm for pCHIS, pCABOL, and pCDAB system

respectively, the thicknesses decreased to 135, 55, and 54 nm respectively after incubation under physiological conditions.

Although Fig. 4 only shows the release based on the percentage of released DNA content, the rearrangement in these multilayered constructs may actually result in the burst release of *not* the naked DNA, but a *complex* composed of DNA and polymer. Following a 1 h incubation of a pCHIS-(CTDNA#pCHIS)₁₀ multilayers in PBS medium pH 7.4, dynamic light scattering measurements revealed the presence of polydisperse (PDI ~1) particles in the size range of ~700 nm. Polyplexes are usually formed and measured at a specific polymer/DNA weight ratio in medium without salt. However, despite the initial homogenous particle sizes, polyplexes are also

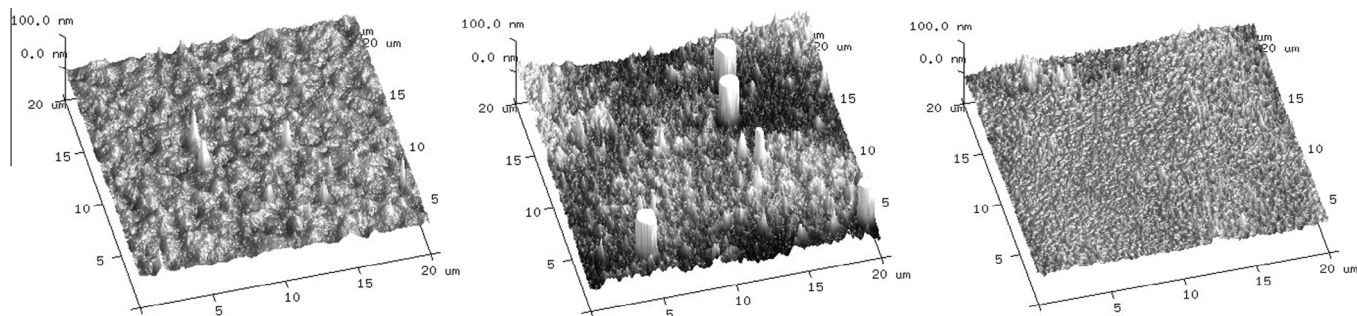


Fig. 5. Surface profiles of (from left to right) pCHIS-(CTDNA#pCHIS)₁₀, pCABOL-(CTDNA#pCABOL)₁₀, and pCDAB-(CTDNA#pCDAB)₁₀ multilayers after being incubated in PBS buffer pH 7.4 at 37 °C shown using the same height scaling as that used in Table 2 (max z-axis value = 100 nm).

known to become unstable upon mixing with serum-containing cell culture medium in which transfections are carried out [51]. Similarly, the thicker multilayers fabricated in this study undergo rearrangement in the presence of cell culture medium, releasing materials that are likely thermodynamically stable complexes of DNA and polymer. It is therefore expected that these films are able to induce transfection at least through the released polymer/DNA complexes.

3.6. *In vitro* reductive degradation of multilayered thin films

Owing to the presence of disulfide bonds in the main chain of the three PAAs used to build multilayers, the resulting multilayers have reducible properties. However, due to the structural differences between the three PAAs the respective films may show different stability profiles under the same reducing conditions. Furthermore, a similar PAA lacking disulfide linkages may also be used to serve as a negative control to verify that the observed degradation is indeed due to the presence of disulfide bonds in the main chain of the PAAs. In this study, pMDAB (synthesized with *N,N*-methylene bisacrylamide (MBA) instead of the disulfide-containing CBA) was used as the non-reducible counterpart of pCDAB.

To investigate the degradability of the multilayers, films were incubated in a solution of 1.0 mM DTT in PBS buffer at pH 7.4. The

degradation profiles for pCHIS-(CTDNA#pCHIS)₁₀ and pCDAB-(CTDNA#pCDAB)₁₀ are shown in Fig. 6. Profiles of pCHIS-(CTDNA#pCHIS)₁₀ and pCDAB-(CTDNA#pCDAB)₁₀ in PBS buffer at pH 7.4 without DTT are shown for comparison. The pCABOL-(CTDNA#pCABOL)₁₀ films degrade substantially faster than the other multilayers and practically no film was left already after the first minute of incubation under reducing conditions (data not shown). The control pMDAB system exposed to the same reducing conditions displayed a similar stability profile as the pCDAB system treated without DTT, confirming that the degradation was indeed caused by the reduction of disulfide bonds.

Fig. 6 shows that the investigated multilayers undergo rapid degradation in the presence of 1 mM of DTT under physiological conditions. From the observed degradation trend pCABOL > pCHIS > pCDAB, it can be proposed that degradation is enhanced by the higher porosity (looser structure) induced by the thermodynamic rearrangement of the thicker films. The higher porosity promotes diffusion of negatively-charged DTT into the lower parts of the multilayered systems causing more rapid reduction and break down of the films.

It has been previously reported that the cellular membrane may contain reducing enzymes capable of degrading multilayered thin films on which the cells were growing [25,26]. Although to the best of our knowledge no quantitative study has been reported on the reducing strength of the cellular membrane, the 1 mM

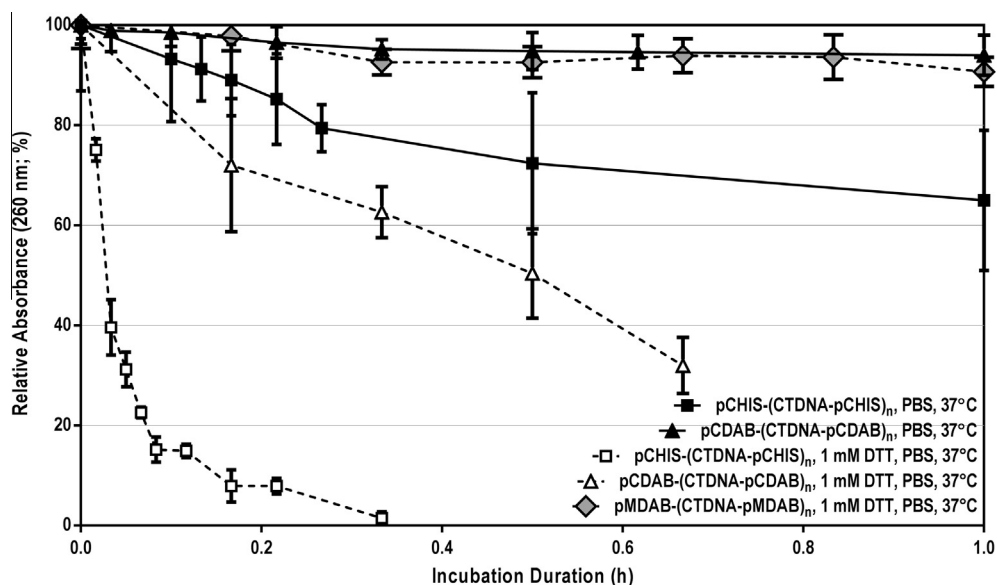


Fig. 6. Degradation profiles of pCHIS-(CTDNA#pCHIS)₁₀ and pCDAB-(CTDNA#pCDAB)₁₀ multilayers with and without the presence of 1 mM DTT in PBS buffer pH 7.4 at 37 °C. Relative absorbance values are shown by normalizing the corrected absorbance values at every time point to that of time 0.

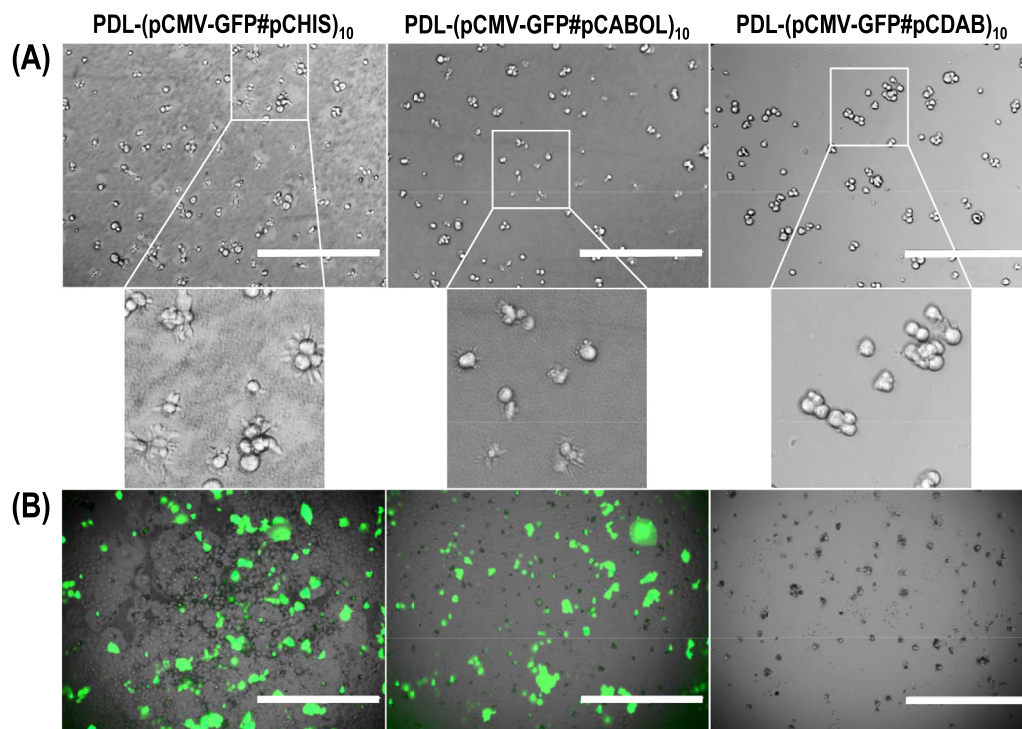


Fig. 7. (A) Light microscopy images of COS-7 cells 6 h after seeding on the three different multilayers at 10× magnification (bars = 400 μm); (B) overlay of GFP fluorescence and light microscope images of COS-7 cells seeded on the same multilayers after 48 h of culture at 4× magnification (bars = 400 μm).

concentration of DTT in the degradation solution can be predicted to be much higher. The reduction provided by the cellular membrane is more highly localized and therefore may not result in as high a degradation rate as that achievable if all the reducing agents are dissolved and distributed evenly in the solution. Nevertheless, for the particular multilayer thin films reported in this study, the effect of rearrangement induced by physiological salt concentration may have been more detrimental in payload (i.e., DNA) release than the extracellular reducing microenvironment of the cells.

3.7. Cell viability and transfection on multilayered thin films

To investigate whether cells are able to attach and proliferate, and are susceptible to transfection, when grown on multilayers, functional plasmid DNA (pCMV-GFP) encoding for GFP was used to substitute for the inexpensive CTDNA that had been used to study the characteristics of multilayer build-up, DNA release, degradation, wettability, and surface profiles. Poly-D-lysine-coated 96 well plates (PDL-TCPS, commercially available) were used as the substrate for multilayer build-up to facilitate handling and cell distribution. Albeit no characterization was conducted on multilayers built in these wells, confirmation of multilayer formation is usually easily detected by light microscopy readily available in cell culture laboratories. As further control, the multilayers PAA-(pCMV-GFP#PAA)₁₀ built on glass substrates have also been used for the same *in vitro* viability and transfection efficiency study with similar results qualitatively. It is therefore believed that the difference in the identity of the precursor layer (PAA versus PDL) does not significantly affect the performance of multilayers.

COS-7 cells were seeded on multilayer-coated PDL-TCPS wells at a seeding density of 4500 cells/well for 96 well plates (i.e., ~13,000 cells/cm²). Initial cell attachment and morphology were monitored 6 h after seeding by light microscopy. Microscopy images of COS-7 cells seeded on different surfaces are shown in Fig. 7.

Fig. 7a shows that the pCHIS-based system provides best cell attachment followed by the pCABOL-based multilayer. pCDAB-

based films on the other hand, impede COS-7 cell attachment as observed by the rounded morphology of the cells. On this latter system, cells tend to aggregate rather than attaching to the surface regardless of the high positive charge on the surface. Fig. 7A also shows a rough surface profile of the pCHIS system, owing to the thickness of the multilayer. After 48 h, the cells were further imaged for GFP expression. Fig. 7B shows representative overlay images of the cells cultured on the three different films after 2 days of culture.

From Fig. 7B, it can be seen that the PDL-(pCMV-GFP#pCABOL)₁₀ and PDL-(pCMV-GFP#pCHIS)₁₀ multilayers are able to transfect cells, whereas the PDL-(pCMV-GFP#pCDAB)₁₀ did not display transfection. The extent of cell transfection is optimal after 2 days of culture. Qualitative observation at day three did not show significant increases in transfection (data not shown). Upon closer investigation of the cell morphology at these later time points, it becomes apparent that the PDL-(pCMV-GFP#pCDAB)₁₀ system suppresses cell attachment and proliferation. This was further confirmed by

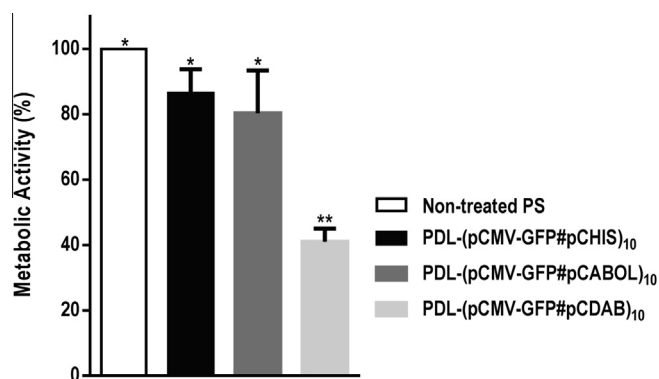


Fig. 8. Metabolic activity of COS-7 cells cultured on various multilayered surfaces relative to PS control. * Not significantly different from one another ($p > 0.05$), ** significantly different from the rest of the data ($p < 0.05$).

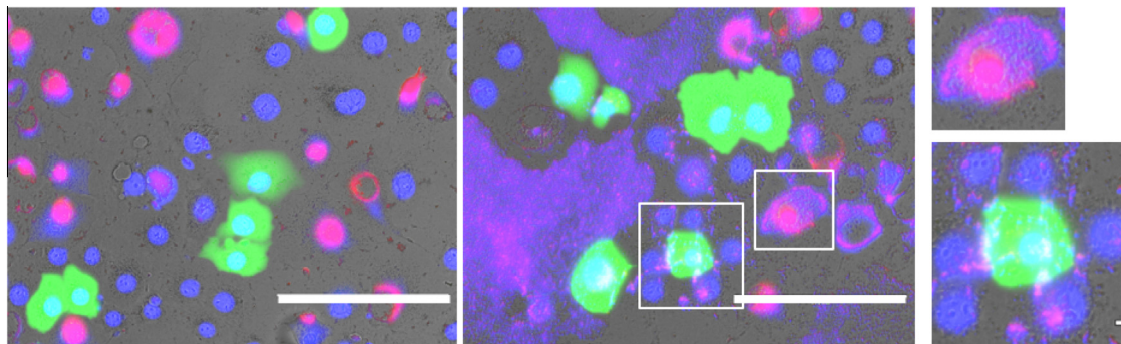


Fig. 9. Representative overlay images of COS-7 cells stained with Hoechst 33258 (blue, live) and EthD-1 (red, dead) after 2 days of culture on top of PDL-(pCMV-GFP#pCABOL)₁₀ (left) and PDL-(pCMV-GFP#pCHIS)₁₀ (right) at 20× magnification. Bars = 200 μm.

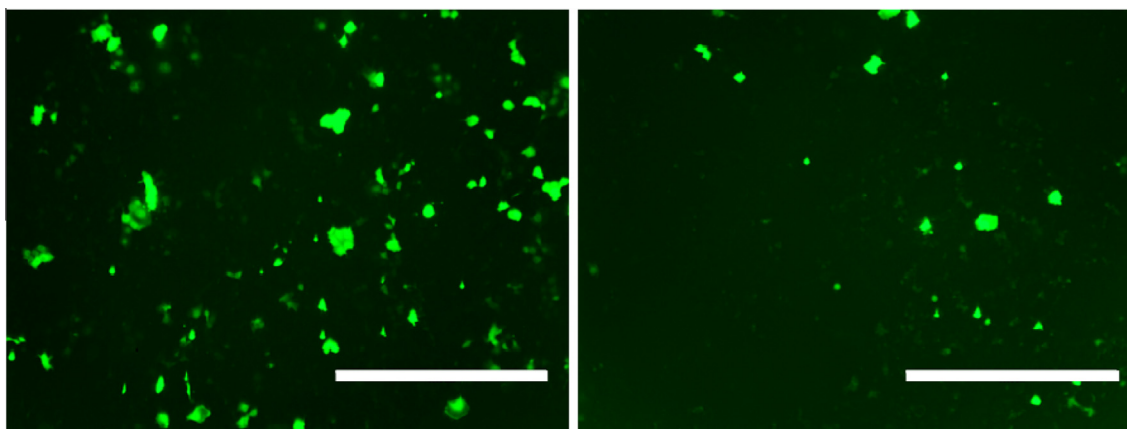


Fig. 10. Representative GFP fluorescence images of COS-7 cells seeded on top of “unwashed” (left) and “washed” (right) PDL-(pCMV-GFP#pCHIS)₁₀ multilayer after 48 h of culture. Images were at 4× magnification (scale bar = 1000 μm).

performing the AlamarBlue assay to quantitatively assess metabolic activity of cells cultured on the different surfaces after 2 days. The fluorescence intensity of metabolically-reduced resazurin is shown in Fig. 8 as % metabolic activity relative to cells cultured on PS control. This Figure indicates that COS-7 cells were able to proliferate to similar extents on pCABOL-based and pCHIS-based multilayers as well as on non-tissue culture treated PS surfaces. On the other hand, pCDAB-based multilayer displayed significantly poorer COS-7 cell proliferation, confirming higher cytotoxicity, most likely due to the higher amount of cationic charges on this polymer as further corroborated by the cell morphology shown in Fig. 7A.

The metabolic activity of transfected cells shown in Fig. 8 was further assessed qualitatively by staining the cells with Hoechst 33258 (blue) and EthD-1 (red) for both live and dead cells, respectively. Representative overlay images of transfected cells on pCABOL and pCHIS-based systems are shown in Fig. 9. In both systems, the detected transfected cells stained negative for EthD-1, indicating good viability with well-defined nuclei. Further, the rough features that have been persistently observed for pCHIS samples (see Fig. 7) can now be seen to stain positive for both Hoechst 33258 and EthD-1, staining for DNA. These features are most likely visible fragments of released polymer-DNA complexes. This is most likely possible due to the thick nature of the pCHIS films compared to the thinner pCABOL films.

In order to further understand the effect of rapid release on transfection efficiency, as discussed earlier, an experiment was carried out in which COS-7 cells were seeded with the same seeding density on regular “unwashed” pCHIS films and “washed” pCHIS films. The extent of GFP expression on both systems after 2 days of culture is represented in Fig. 10. In general, transfection

efficiency was much lower for the “washed” system than for the “unwashed” system which indicates that the fast initial release results in the release of transfection agent. Further, to assess whether the released transfection agent is still active for transfection, cell culture medium that has been used to incubate multilayers without cells under physiological conditions for 1 h was added to cells cultured on a non-multilayer-coated surface and the extent of transfection was observed after 2 days of culture. Interestingly, no transfection was observed (data not shown). It is possible that the released transfection agent became deactivated/degraded upon contact with cell culture medium albeit only for 1 h. This result signifies the necessity of direct contact between the multilayers and the cells to be treated. This direct contact possibly encourages a rapid intracellular uptake of active transfection agents through a restriction of space.

Under the employed conditions, a transfection efficiency of approximately 11% was observed. In a separate study, we have optimized transfection efficiency in relation to cell seeding density, bilayer number, and identity of topmost layer [52]. These studies revealed optimum transfection at a cell seeding of 7360 cells/well (slightly higher than the 4500 cells/well employed in this study), with FACS analysis revealing efficiencies of 45% and 30% for pCABOL and pCHIS multilayers at 10 bilayers. For pCDAB systems, at any seeding density, no transfection was observed.

4. Conclusions

Poly(amido amine)s, being peptidomimetic polymers with inherent positive charge under physiological conditions, show

good interaction with DNA and readily form multilayered thin films. Three bioreducible poly(amido amine)s with different side chains show different layer build-up profiles and film properties. For all three systems, uniform coverage was obtained after at least 4 deposition cycles and throughout the deposition cycles the build-up of 10 bilayers progressed in a linear manner. Thicker multilayers with higher material deposition were obtained from pCHIS (containing imidazole moieties in the polymer side chains) and pCABOL (containing primary alcohols in the polymer side chains) polymers, while pCDAB (containing primary amines in the polymer side chains) having the highest cationic charge density was found to lead to the thinnest films with the lowest material deposition. The polymers pCABOL and pCHIS with less, yet still sufficient, positive charges gave rise to a rougher structure, providing more surface area for the counter polyelectrolyte (in this case DNA) to deposit onto, while more positively-charged polymer (pCDAB) tends to deposit a more compact layer, providing less area for the incoming counter polyelectrolyte. Ultraviolet spectroscopy data of the layers were in good agreement with thickness measurement via atomic force microscopy. At 10 bilayers, both pCHIS and pCABOL-based multilayers incorporated a relatively similar amount of DNA. However, pCHIS-based films were much thicker, possibly indicating higher polymer to DNA ratio than pCABOL-based films.

In the presence of physiological salt concentration, the thicker pCABOL- and pCHIS-based films were found to rapidly release film components (i.e., approximately half of initial DNA content within 1 h), most likely in the form of polymer-DNA complexes. *In vitro* cell experiments with COS-7 cells demonstrate that pCABOL- and pCHIS-based multilayered systems can facilitate cell attachment and proliferation. However, the pCDAB-based multilayer, which is very stable under physiological conditions, displayed only limited cell attachment and higher cytotoxicity, most likely due to the higher cationic charge density of this polymer. Out of the three different polymers, pCABOL- and pCHIS-based multilayered systems were able to transfect COS-7 cells cultured on top of the multilayers containing plasmids encoding for GFP after 2 days of incubation. In this study transfection efficiencies of up to 11% of the total COS-7 cells cultured on pCABOL- and pCHIS-based multilayers were observed qualitatively.

In conclusion multilayers from poly(amido amine)s and DNA offer the possibility to endow surfaces with cell-transfecting capabilities. To this purpose, a release mechanism is necessary to release DNA in a transfection-active formulation. We have observed from this study that a burst release mechanism as observed for pCABOL- and pCHIS-based films may help transfection to a rapid early start. We believe that the multilayered systems presented in this study hold great potential to be used as cell-transfecting coatings for various biomaterials in biomedical applications.

Acknowledgements

This work was supported by a grant from the Dutch government to the Netherlands Institute for Regenerative Medicine (NIRM project to S.D.H.). Mrs. Hetty ten Hoopen is kindly acknowledged for AFM measurements.

Appendix A. Figures with essential color discrimination

Certain figures in this article, particularly Figs. 7, 9 and 10, are difficult to interpret in black and white. The full color images can be found in the on-line version, at <http://dx.doi.org/10.1016/j.actbio.2015.04.022>.

Appendix B. Supplementary data

Supplementary data associated with this article can be found, in the online version, at <http://dx.doi.org/10.1016/j.actbio.2015.04.022>.

References

- [1] Ariga K, Ji QM, Hill JP, Bando Y, Aono M. Forming nanomaterials as layered functional structures toward materials nanoarchitectonics. *NPG Asia Mater* 2012;4:1884–4049.
- [2] Hammond PT. Building biomedical materials layer-by-layer. *Mater Today* 2012;15:196–206.
- [3] van den Beucken JJ, Walboomers XF, Vos MR, Sommerdijk NA, Nolte RJ, Jansen JA. Biological responses to multilayered DNA-coatings. *J Biomed Mater Res B Appl Biomater* 2007;81:231–8.
- [4] De Koker S, De Cock LJ, Rivera-Gil P, Parak WJ, Auzely Veltz R, Vervaeet C, et al. Polymeric multilayer capsules delivering biotherapeutics. *Adv Drug Deliv Rev* 2011;63:748–61.
- [5] Jewell CM, Zhang J, Fredin NJ, Wolff MR, Hacker TA, Lynn DM. Release of plasmid DNA from intravascular stents coated with ultrathin multilayered polyelectrolyte films. *Biomacromolecules* 2006;7:2483–91.
- [6] Saurer EM, Flessner RM, Sullivan SP, Prausnitz MR, Lynn DM. Layer-by-layer assembly of DNA- and protein-containing films on microneedles for drug delivery to the skin. *Biomacromolecules* 2010;11:3136–43.
- [7] Saurer EM, Jewell CM, Kuchenreuther JM, Lynn DM. Assembly of erodible, DNA-containing thin films on the surfaces of polymer microparticles: toward a layer-by-layer approach to the delivery of DNA to antigen-presenting cells. *Acta Biomater* 2009;5:913–24.
- [8] Weiner GJ, Liu HM, Wooldridge JE, Dahle CE, Krieg AM. Immunostimulatory oligodeoxynucleotides containing the CpG motif are effective as immune adjuvants in tumor antigen immunization. *Proc Natl Acad Sci U S A* 1997;94:10833–7.
- [9] Vollmer J, Weeratna R, Payette P, Jurk M, Schetter C, Laucht M, et al. Characterization of three CpG oligodeoxynucleotide classes with distinct immunostimulatory activities. *Eur J Immunol* 2004;34:251–62.
- [10] Hu Y, Cai K, Luo Z, Zhang R, Yang L, Deng L, et al. Surface mediated in situ differentiation of mesenchymal stem cells on gene-functionalized titanium films fabricated by layer-by-layer technique. *Biomaterials* 2009;30:3626–35.
- [11] Yamauchi F, Kato K, Iwata H. Layer-by-layer assembly of poly(ethyleneimine) and plasmid DNA onto transparent indium-tin oxide electrodes for temporally and spatially specific gene transfer. *Langmuir* 2005;21:8360–7.
- [12] Lvov Y, Decher G, Sukhorukov G. Assembly of thin-films by means of successive deposition of alternate layers of DNA and poly(allylamine). *Macromolecules* 1993;26:5396–9.
- [13] Richard D, Nguyen I, Affolter C, Meyer F, Schaaf P, Voegel JC, et al. Polyelectrolyte multilayer-mediated gene delivery for semaphorin signaling pathway control. *Small* 2010;6:2405–11.
- [14] Zhang JT, Chua LS, Lynn DM. Multilayered thin films that sustain the release of functional DNA under physiological conditions. *Langmuir* 2004;20:8015–21.
- [15] Ray K, Badugu R, Lakowicz JR. Polyelectrolyte layer-by-layer assembly to control the distance between fluorophores and plasmonic nanostructures. *Chem Mater* 2007;19:5902–9.
- [16] DeMuth PC, Moon JJ, Suh H, Hammond PT, Irvine DJ. Releasable layer-by-layer assembly of stabilized lipid nanocapsules on microneedles for enhanced transcutaneous vaccine delivery. *ACS Nano* 2012;6:8041–51.
- [17] Jiang QH, Liu L, Shen JW, Peel S, Yang GL, Zhao SF, et al. Influence of multilayer rhBMP-2 DNA coating on the proliferation and differentiation of MC3T3-E1 cells seeded on roughed titanium surface. *J Biomed Mater Res A* 2012;100:2766–74.
- [18] Lin QK, Ren KF, Ji J. Hyaluronic acid and chitosan-DNA complex multilayered thin film as surface-mediated nonviral gene delivery system. *Colloids Surf B* 2009;74:298–303.
- [19] Meyer F, Ball V, Schaaf P, Voegel JC, Ogier J. Polyplex-embedding in polyelectrolyte multilayers for gene delivery. *Biochim Biophys Acta* 2006;1758:419–22.
- [20] Coue G, Freese C, Unger RE, Kirkpatrick CJ, Engbersen JF. Bioresponsive poly(amidoamine)s designed for intracellular protein delivery. *Acta Biomater* 2013;9:6062–74.
- [21] Lin C, Blaauboer CJ, Timoneda MM, Lok MC, van Steenberg M, Hennink WE, et al. Bioreducible poly(amido amine)s with oligoamine side chains: synthesis, characterization, and structural effects on gene delivery. *J Control Release* 2008;126:166–74.
- [22] Lin C, Engbersen JF. Effect of chemical functionalities in poly(amido amine)s for non-viral gene transfection. *J Control Release* 2008;132:267–72.
- [23] Piest M, Lin C, Mateos-Timoneda MA, Lok MC, Hennink WE, Feijen J, et al. Novel poly(amido amine)s with bioreducible disulfide linkages in their diamino-units: structure effects and in vitro gene transfer properties. *J Control Release* 2008;132:E12–3.
- [24] van der Aa LJ, Vader P, Storm G, Schifflers RM, Engbersen JF. Optimization of poly(amido amine)s as vectors for siRNA delivery. *J Control Release* 2011;150:177–86.
- [25] Donoghue N, Yam PT, Jiang XM, Hogg PJ. Presence of closely spaced protein thiols on the surface of mammalian cells. *Protein Sci* 2000;9:2436–45.

- [26] Sahaf B, Heydari K, Herzenberg LA, Herzenberg LA. The extracellular microenvironment plays a key role in regulating the redox status of cell surface proteins in HIV-infected subjects. *Arch Biochem Biophys* 2005;434:26–32.
- [27] Luo D, Saltzman WM. Enhancement of transfection by physical concentration of DNA at the cell surface. *Nat Biotechnol* 2000;18:893–5.
- [28] Segura T, Volk MJ, Shea LD. Substrate-mediated DNA delivery: role of the cationic polymer structure and extent of modification. *J Control Release* 2003;93:69–84.
- [29] Shen H, Tan J, Saltzman WM. Surface-mediated gene transfer from nanocomposites of controlled texture. *Nat Mater* 2004;3:569–74.
- [30] Blacklock J, Handa H, Soundara Manickam D, Mao G, Mukhopadhyay A, Oupicky D. Disassembly of layer-by-layer films of plasmid DNA and reducible TAT polypeptide. *Biomaterials* 2007;28:117–24.
- [31] Blacklock J, You YZ, Zhou QH, Mao G, Oupicky D. Gene delivery in vitro and in vivo from bioreducible multilayered polyelectrolyte films of plasmid DNA. *Biomaterials* 2009;30:939–50.
- [32] Redolfi Riva E, Desii A, Sartini S, La Motta C, Mazzolai B, Mattoli V. PMMA/polysaccharides nanofilm loaded with adenosine deaminase inhibitor for targeted anti-inflammatory drug delivery. *Langmuir* 2013;29:13190–7.
- [33] Wood KC, Chuang HF, Batten RD, Lynn DM, Hammond PT. Controlling interlayer diffusion to achieve sustained, multiagent delivery from layer-by-layer thin films. *Proc Natl Acad Sci U S A* 2006;103:10207–12.
- [34] Kim B-S, Lee H-I, Min Y, Poon Z, Hammond PT. Hydrogen-bonded multilayer of pH-responsive polymeric micelles with tannic acid for surface drug delivery. *Chem Commun* 2009:4194–6.
- [35] Schmidt DJ, Moskowitz JS, Hammond PT. Electrically triggered release of a small molecule drug from a polyelectrolyte multilayer coating. *Chem Mater* 2010;22:6416–25.
- [36] Bechler SL, Lynn DM. Characterization of degradable polyelectrolyte multilayers fabricated using DNA and a fluorescently-labeled poly(β -amino ester): shedding light on the role of the cationic polymer in promoting surface-mediated gene delivery. *Biomacromolecules* 2012;13:542–52.
- [37] Zintchenko A, van der Aa LJ, Engbersen JF. Improved synthesis strategy of poly(amidoamine)s for biomedical applications: catalysis by “green” biocompatible earth alkaline metal salts. *Macromol Rapid Commun* 2011;32:321–5.
- [38] Kim ST, Saha K, Kim C, Rotello VM. The role of surface functionality in determining nanoparticle cytotoxicity. *Acc Chem Res* 2013;46:681–91.
- [39] Picart C, Mutterer J, Richert L, Luo Y, Prestwich GD, Schaaf P, et al. Molecular basis for the explanation of the exponential growth of polyelectrolyte multilayers. *Proc Natl Acad Sci U S A* 2002;99:12531–5.
- [40] Decher G, Schmitt J. Fine-tuning of the film thickness of ultrathin multilayer films composed of consecutively alternating layers of anionic and cationic polyelectrolytes. In: Helm C, Lösche M, Möhwald H, editors. *Trends in colloid and interface science VI*. Steinkopff; 1992. p. 160–4.
- [41] Shiratori SS, Rubner MF. pH-dependent thickness behavior of sequentially adsorbed layers of weak polyelectrolytes. *Macromolecules* 2000;33:4213–9.
- [42] Park SY, Rubner MF, Mayes AM. Free energy model for layer-by-layer processing of polyelectrolyte multilayer films. *Langmuir* 2002;18:9600–4.
- [43] Cai K, Hu Y, Wang Y, Yang L. Build up of multilayered thin films with chitosan/DNA pairs on poly(D, L-lactic acid) films: physical chemistry and sustained release behavior. *J Biomed Mater Res A* 2008;84:516–22.
- [44] Ruiz-Chica AJ, Soriano A, Tunon I, Sanchez-jimenez FM, Silla E, Ramirez FJ. FT-Raman and QM/MM study of the interaction between histamine and DNA. *Chem Phys* 2006;324:579–90.
- [45] Ladam G, Schaad P, Voegel JC, Schaaf P, Decher G, Cuisinier F. In situ determination of the structural properties of initially deposited polyelectrolyte multilayers. *Langmuir* 2000;16:1249–55.
- [46] Ren KF, Wang YX, Ji J, Lin QK, Shen JC. Construction and deconstruction of PLL/DNA multilayered films for DNA delivery: effect of ionic strength. *Colloids Surf B* 2005;46:63–9.
- [47] Schüler C, Caruso F. Decomposable hollow biopolymer-based capsules. *Biomacromolecules* 2001;2:921–6.
- [48] Nolte AJ, Takane N, Hindman E, Gaynor W, Rubner MF, Cohen RE. Thin film thickness gradients and spatial patterning via salt etching of polyelectrolyte multilayers. *Macromolecules* 2007;40:5479–86.
- [49] Mjahed H, Voegel J-C, Senger B, Chassepot A, Rameau A, Ball V, et al. Hole formation induced by ionic strength increase in exponentially growing multilayer films. *Soft Matter* 2009;5:2269–76.
- [50] Tokuda Y, Miyagishima T, Tomida K, Wang B, Takahashi S, Sato K, et al. Dual pH-sensitive layer-by-layer films containing amphoteric poly(diallylamine-co-maleic acid). *J Colloid Interface Sci* 2013;399:26–32.
- [51] Dash PR, Read ML, Barrett LB, Wolfert MA, Seymour LW. Factors affecting blood clearance and in vivo distribution of polyelectrolyte complexes for gene delivery. *Gene Ther* 1999;6:643–50.
- [52] Hujaya SD, Marchioli G, Roelofs K, van Apeldoorn AA, Moroni L, Karperien M, et al. Poly(amido amine)-based multilayered thin films on 2D and 3D supports for surface-mediated cell transfection. *J Control Release* 2015(205):181–9.